J. Materials, Conc. Struct., Pavements, JSCE, No.662/V-49, 231-245, 2000 November

# SHEAR TRANSFER ALONG FRP-CONCRETE INTERFACE IN FLEXURAL MEMBERS

Zhishen WU[1] and Hedong NIU[2]

[1]Member of JSCE, Dr. Eng., Associate Professor, Department of Urban & Civil Engineering, Ibaraki University (Nakanarusawa 4-12-1, Hitachi 316-8511, Japan)
[2]Student Member of JSCE, M. Eng., Dr. Candidate, Department of Urban & Civil Engineering, Ibaraki University (Nakanarusawa 4-12-1, Hitachi 316-8511, Japan)

With the increasing use of Fiber Reinforced Polymer (FRP) composites as external reinforcement in the rehabilitation and retrofit of existing concrete structures, more and more attention has been paid to the performance of FRP-concrete interface, which is susceptible to debonding or peeling-off due to stress concentrations or bond imperfections. In this paper, the effects of flexural cracks of concrete on interfacial shear stresses in FRP-strengthened R/C beams are investigated for several load cases based on linear elastic beam theories. Through theoretical analyses and investigations on available existing experimental data, a methodology is also proposed for predicting the debonding initiation load due to flexural cracks.

*Key Words : FRP composites, interfacial stress, flexural crack, initial debonding, fracture energy*

## 1. INTRODUCTION

Fiber Reinforced Polymer (FRP) composites have been increasingly used as external reinforcement in lieu of their steel counterparts in the rehabilitation and retrofit of existing concrete structures due to their much more beneficial characteristics such as ease in handling, resistance to corrosion, light weight and high strength. The pivot to the reinforcement effect of FRP-strengthened concrete structures is the performance of FRP-concrete interface, which is susceptible to debonding and peeling-off due to stress concentrations or bond imperfections. The local fractures, such as the interfacial crack propagation initiated from the ends of flexural cracks of concrete, the peeling-off initiated from the ends of shear cracks of concrete and the delamination initiated from curtailment zone of steel/FRP plates or sheets, often lead to premature failure of strengthened beams[1), 2), 3), 4)], to which more and more attention has been paid in recent years.

Considerable researches have been directed to investigate the phenomenon of shear and normal stress concentrations at the cut-off point of steel/FRP plates and develop the corresponding failure criteria for predicting the premature failure load for steel/FRP-strengthened beams[5), 6), 7), 8), 9), 10)]. Roberts[5)] developed a simple approximate expression for predicting the shear and normal stress concentrations in the adhesive layer of RC beams strengthened with steel/FRP plates. Ziraba et al.[6)] proposed a new expression for the peak interface shear and peeling stresses and a predicator equation for shear resistance of RC beam strengthened with FRP plates. Considering that there is a biaxial tensile stress state at the plate curtailment zone, the authors applied the fracture criterion of Mohr-Coulomb to prevent the premature interface failure. Quantrill et al.[7)] calculated the stress level at the plate ends from experimental results using Roberts's formula and got the premature failure criteria for GFRP and CFRP plates, respectively. Using the criteria to predict the premature failure loads did not yield a consistent relationship with the experimental results[10)]. Täljsten[8)] presented an analytical method for calculating the stresses in the adhesive layer using linear elastic theory. The results of the solution were compared with the ones of a finite element analysis. However, the author did not suggest any failure model for calculating the failure load and took no account of shear concentrations at the end of flexural cracks of concrete. Malek et al.[9)] mainly focused on the local failure in concrete beams due to the stress concentrations at the plate ends although they also considered the debonding of the plate at locations of flexural cracks. El-Mihilmy[10)] reviewed a lot of literatures, developed a design procedure based on strain compatibility for analyzing and designing

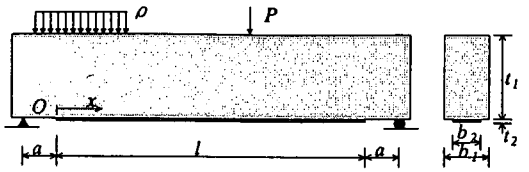


**Fig. 1** Simply supported beam strengthened with FRP

FRP-strengthened reinforced concrete beams and a simplified equation for predicting the premature failure load due to stress concentrations at the plate ends. He recommended that future investigations should be required to develop criteria for the premature failure modes such as debonding due to the flexural cracks in the maximum moment region. The peeling initiated from shear cracks of concrete can be prevented by a rational design and much research work on this area has been done[10]. As stated above, there are few studies concerned with the premature failure mode such as debonding initiated at the flexural cracks in the maximum moment region. Moreover, among the different premature failures of FRP sheets, the debonding and peeling induced by flexural and shear cracks of concrete respectively are considered to be more dominant than the delamination induced by stress concentrations at curtailment zone because the thickness of FRP sheets is much thinner than that of plates. Initiation of debonding due to flexural cracks will affect the structural deformation, degrade the load-carrying capacity, even result in final debonding failure. Therefore determination of initial debonding and calculation of the corresponding load are of great importance to performance evaluation and design of FRP-strengthened concrete structures.

This paper focuses on the development of an analytical method on calculating the interfacial shear and normal stresses due to flexural cracks in FRP-strengthened R/C beams based on the work done by Täljsten[8]. A parametric study is conducted to investigate the effects of design variables such as thickness, width and elastic modulus of FRP sheets and adhesive layer on the distribution of shear stress. And how to predict the initial debonding load is also proposed on the basis of the theoretical analyses and the experimental results.

## 2. THEORETICAL DERIVATION

A differential section, $dx$, can be cut out from a FRP-strengthened beam (**Fig. 1**), as shown in **Fig. 2**. The beam is made from three materials: concrete (or reinforced concrete), adhesive layer and external reinforcement. In the present analysis, the adhesive is

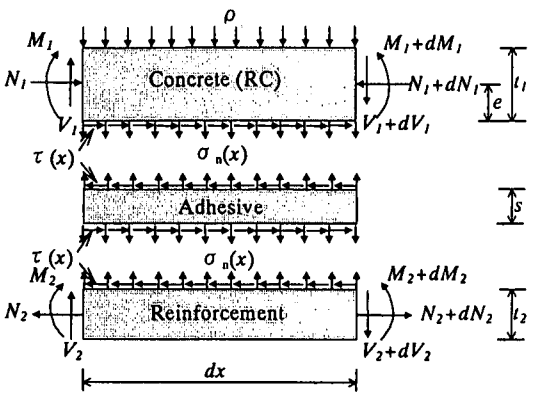


**Fig. 2** Forces in infinitesimal element of composite beam

assumed to only play a role in transferring the stresses from the concrete to FRP reinforcement and the stresses in the adhesive layer do not change through the direction of the thickness.

**(1) Basic equation of elasticity**

The strains $\varepsilon_1(x)$ and $\varepsilon_2(x)$ in the concrete and the external reinforcement near the adhesive interface can be expressed, respectively:

$$\varepsilon_1(x) = \frac{du_1(x)}{dx} = \frac{M_1(x)}{E_1 W_1} - \frac{N_1(x)}{E_1 A_1} \tag{1}$$

$$\varepsilon_2(x) = \frac{du_2(x)}{dx} = \frac{N_2(x)}{E_2 A_2} - \frac{M_2(x)}{E_2 W_2} \tag{2}$$

where $u_1(x)$ and $u_2(x)$ are horizontal displacements of the concrete and the external reinforcement near the adhesive interface, respectively; $M_1(x)$ and $M_2(x)$ are bending moments applied in the concrete and the external reinforcement, respectively; $E_1$ and $E_2$ are Young's moduli of the concrete and the external reinforcement, respectively; $W_1$ and $W_2$ are section moduli of R/C beam based on the concrete and the external reinforcement, respectively; $N_1$ and $N_2$ are axial forces applied in the concrete and the external reinforcement, respectively; $A_1$ and $A_2$ are section areas of the concrete and the external reinforcement, respectively.

And by adopting the equilibrium conditions of the concrete, we have:

$$\text{Along x-direction: } \frac{dN_1(x)}{dx} = \tau(x) b_2 \tag{3}$$

where $\tau(x)$ is shear stress in the adhesive layer and $b_2$ is width of the external reinforcement.

Along z-direction: $\frac{dV_1(x)}{dx} = -[\sigma_n(x)b_2 + \rho b_1]$ (4)

where $V_1(x)$ is shear force applied in the concrete; $\sigma_n(x)$ is normal stress in the adhesive layer; $\rho$ is distributed load per unit area on the R/C beam and $b_1$ is width of R/C beam.

Moment equilibrium: $\frac{dM_1(x)}{dx} = V_1(x) - \tau(x)b_2 e$ (5)

where $e$ is distance from the neutral axis to the bottom of R/C beam.

The equilibrium of the external reinforcement along x-, z- direction and moment equilibrium can be also written as:

Along x-direction: $\frac{dN_2(x)}{dx} = \tau(x)b_2$ (6)

Along z-direction: $\frac{dV_2(x)}{dx} = \sigma_n(x)b_2$ (7)

Moment equilibrium:

$$\frac{dM_2(x)}{dx} = V_2(x) - \tau(x)b_2 t_2/2 \quad (8)$$

where $V_2(x)$ is shear force applied in the external reinforcement and $t_2$ is thickness of the external reinforcement.

**(2) Shear stress distribution along the FRP-concrete interface**

Here, it is considered that the bending stiffness of the external reinforcement is far less than that of the beam to be strengthened and the bending moment in the external reinforcement can be neglected for simplicity in the derivation of shear stress. On the basis of the work done by Täljsten[8] where the author only focused on the cut-off point of the plate and did not take any concrete crack or failure model into consideration, the interfacial shear stresses due to flexural cracks are derived in this section.

The shear stress in the adhesive can be expressed as follows:

$$\tau(x) = K_s \Delta u(x) = K_s[u_2(x) - u_1(x)] \quad (9)$$

where $K_s$ is shear stiffness of the adhesive per unit length and can be deduced as $K_s = \frac{\tau(x)}{\Delta u(x)} = \frac{\tau(x)}{\Delta u(x)/s} \cdot \frac{1}{s} = \frac{G_a}{s}$; $\Delta u(x)$ is relative horizontal displacement at the adhesive interface; $G_a$ is the shear modulus in the adhesive and $s$ is the thickness of the adhesive.

Differentiating equation (9), (1) and (2) with respect to x, respectively, and neglecting the bending moment in the external reinforcement yield:

$$\frac{d\tau(x)}{dx} = K_s\left[\frac{N_2(x)}{E_2A_2} + \frac{N_1(x)}{E_1A_1} - \frac{M_1(x)}{E_1W_1}\right] \quad (10)$$

$$\frac{d^2\tau(x)}{dx^2} = K_s\left[\frac{d^2u_2(x)}{dx^2} - \frac{d^2u_1(x)}{dx^2}\right] \quad (11)$$

where $\frac{d^2u_1(x)}{dx^2} = \frac{1}{E_1W_1}\frac{dM_1(x)}{dx} - \frac{1}{E_1A_1}\frac{dN_1(x)}{dx}$;

$$\frac{d^2u_2(x)}{dx^2} = \frac{1}{E_2A_2}\frac{dN_2(x)}{dx}.$$

Substituting equation (3), (5), (6) into equation (11) gives:

$$\frac{d^2\tau(x)}{dx^2} - \alpha^2\tau(x) + \frac{K_s}{E_1W_1}V_1(x) = 0 \quad (12)$$

where $\alpha^2 = K_s b_2\left[\frac{1}{E_2A_2} + \frac{1}{E_1A_1} + \frac{e}{E_1W_1}\right]$; $V_1(x)$ is shear force at section $x$ due to externally applied loads since the shear force is neglected in the external reinforcement and here it is assumed that the expression of $V_1(x)$ is a linear function of $x$ for the convenience of solution.

The solution to equation (12) is given by:

$$\tau(x) = C_1\cosh(\alpha x) + C_2\sinh(\alpha x) + \frac{K_s}{\alpha^2 E_1W_1}\cdot V_1(x) \quad (13)$$

where $C_1, C_2$ are constants of integration to be determined by the boundary conditions.

Integrating equation (5) with respect to x with the substitution of equation (6) yields:

$$M_1(x) = M(x) - N_2(x)e \quad (14)$$

where $M(x)$ is the bending moment of the composite beam at section x.

Moreover, noticing $N_1(x) = N_2(x)$ and substituting equation (13), (14) into (10) give:

$$\frac{N_2(x)}{b_2} = \frac{1}{\alpha^2}\frac{d\tau(x)}{dx} + \frac{K_s}{\alpha^2}\frac{M(x)}{E_1W_1} \quad (15)$$

In what follows, the closed form solutions for shear stress distribution along the FRP-concrete interface

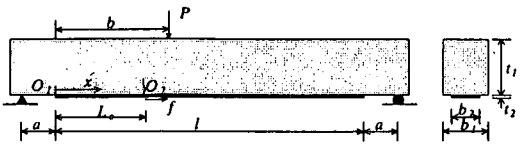

Fig. 3 Three-point bending case with one flexural crack

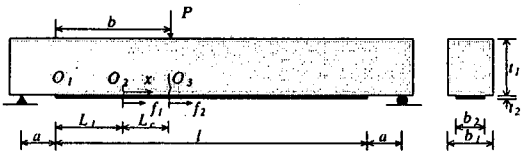

Fig. 4 Three-point bending case with two flexural cracks

due to the flexural cracks are derived for several load cases.

① Three-point bending case

*(a) Interfacial shear stresses due to unique flexural crack*

For three-point bending case (**Fig. 3**), the interfacial shear stresses due to unique flexural crack can be obtained with the following constraints:

$$\begin{cases} N_2(x) = 0 & x = 0 \\ N_2(x) = f & x = L_c \end{cases}$$

$$V_1(x) = \frac{P(l+a-b)}{l+2a} \tag{16}$$

Therefore, from equation (15), we can derive the constants of integration as follows:

$$C_1 = \frac{\frac{K_s}{\alpha E_1 W_1}\{a[\cosh(\alpha L_c)-1]-L_c\}V_1(x)+\frac{\alpha f}{b_2}}{\sinh(\alpha L_c)}$$

$$C_2 = -\frac{K_s a}{\alpha E_1 W_1}\cdot V_1(x) \tag{17}$$

The shear stress distribution in the adhesive layer of FRP-strengthened beam with unique flexural crack can be expressed as:

$$\tau(x) = \frac{K_s P(l+a-b)}{\alpha E_1 W_1 (l+2a)}\left\{a\left[\frac{(\cosh(\alpha L_c)-1)\cosh(\alpha x)}{\sinh(\alpha L_c)} - \sinh(\alpha x)\right] + \frac{1}{\alpha} - \frac{L_c\cosh(\alpha x)}{\sinh(\alpha L_c)}\right\} + \frac{\alpha f\cosh(\alpha x)}{b_2\sinh(\alpha L_c)}$$

$$x \in [0, L_c] \tag{18}$$

*(b) Interfacial shear stresses due to two flexural cracks*

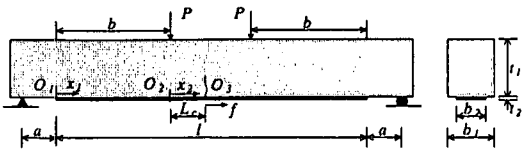

Fig. 5 Four-point bending case with one flexural crack

For the case of two flexural cracks (**Fig. 4**), the interfacial shear stresses can be expressed in two segments. The shear stresses between $O_1$ and $O_2$ can be obtained as stated above. The shear stresses between $O_2$ and $O_3$ can be deduced by the following constraints:

$$\begin{cases} N_2(x) = f_1 & x = 0 \\ N_2(x) = f_2 & x = L_c \end{cases}$$

$$V_1(x) = \frac{P(l+a-b)}{l+2a} \tag{19}$$

Based on equation (15), the constants of integration can be obtained as follows:

$$C_2 = \frac{\alpha f_1}{b_2} - \frac{K_s P(l+a-b)(L_1+a)}{\alpha E_1 W_1 (l+2a)}$$

$$C_1 = \frac{\frac{\alpha f_2}{b_2} - \frac{K_s P(l+a-b)(L_1+a+L_c)}{\alpha E_1 W_1 (l+2a)} - C_2\cosh(\alpha L_c)}{\sinh(\alpha L_c)}$$

$$\tau(x) = C_1\cosh(\alpha x) + C_2\sinh(\alpha x) + \frac{K_s P(l+a-b)}{\alpha^2 E_1 W_1 (l+2a)}$$

$$x \in [0, L_c] \tag{20}$$

② Four-point bending case

For four-point bending case (**Fig. 5**), the constants of integration for interfacial shear stresses in $O_1O_2$ and $O_2O_3$ can be obtained by:

$$\begin{cases} N_2^1(x_1) = 0 & x_1 = 0 \\ N_2^2(x_2) = f & x_2 = L_c \\ \tau^1(x_1) = \tau^2(x_2) & x_1 = b, x_2 = 0 \\ N_2^1(x_1) = N_2^2(x_2) & x_1 = b, x_2 = 0 \end{cases}$$

$$V_1^1(x) = P \qquad V_1^2(x) = 0 \tag{21}$$

where the superscripts, "1" and "2", indicate stresses or forces in $O_1O_2$ and $O_2O_3$, respectively.

The interfacial shear stresses located between $O_1$ and $O_2$ can be written as follows:

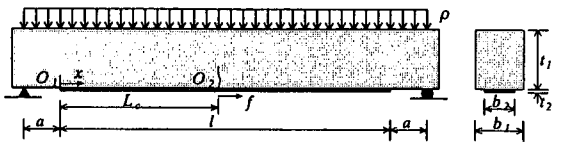


Fig. 6 Uniformly distributed loading case (one flexural crack)

$$C_1^1 = \frac{\frac{\alpha f}{b_2} + \frac{K_s P}{\alpha E_1 W_1}\left\{a\cosh[\alpha(b+L_c)] - \frac{\sinh(\alpha L_c)}{\alpha} - (a+b)\right\}}{\sinh[a(b+L_c)]}$$

$$C_2^1 = -\frac{K_s P a}{\alpha E_1 W_1}]$$

$$\tau^1(x) = C_1^1\cosh(\alpha x) + C_2^1\sinh(\alpha x) + \frac{K_s P}{\alpha^2 E_1 W_1} \quad x \in [0, b] \quad (22)$$

And the interfacial shear stresses located between $O_2$ and $O_3$ can be written as follows:

$$C_1^2 = C_1^1\cosh(\alpha b) + \frac{K_s P}{\alpha E_1 W_1}\left[\frac{1}{\alpha} - a\sinh(\alpha b)\right]$$

$$C_2^2 = C_1^1\sinh(\alpha b) - \frac{K_s P a}{\alpha E_1 W_1}\cosh(\alpha b)$$

$$\tau^2(x) = C_1^2\cosh(\alpha x) + C_2^2\sinh(\alpha x) \quad x \in [0, L_c] \quad (23)$$

③ Uniformly distributed loading case

For the uniformly distributed loading case (**Fig. 6**), the boundary conditions can be written as:

$$\begin{cases} N_2(x) = f_1 & x = 0 \\ N_2(x) = f_2 & x = L_c \end{cases}$$

$$V_1(x) = \rho b_1\left(\frac{l}{2} - x\right) \quad (24)$$

Based on equation (15), the interfacial shear stresses can be obtained as follows:

$$C_2 = -\frac{K_s \rho b_1}{\alpha E_1 W_1}\left[\frac{a(l+a)}{2} - \frac{1}{\alpha^2}\right]$$

$$C_1 = \frac{\frac{\alpha f}{b_2} - C_2\cosh(\alpha L_c) + \frac{K_s \rho b_1}{\alpha E_1 W_1}\left[\frac{1}{\alpha^2} - \frac{(a+L_c)(l+a-L_c)}{2}\right]}{\sinh(\alpha L_c)}$$

$$\tau(x) = C_1\cosh(\alpha x) + C_2\sinh(\alpha x) + \frac{K_s \rho b_1}{\alpha^2 E_1 W_1}\left(\frac{l}{2} - x\right) \quad (25)$$

For all the cases stated above, the maximum shear stress in adhesive layer ignoring the minor terms can be obtained from the following approximate equation:

$$\tau_{\max} = \frac{f}{b_2}\sqrt{\frac{K_s}{E_2 t_2}} \quad (26)$$

**(3) Normal stress distribution along the FRP-concrete interface**

The normal stress in the adhesive can be expressed as follows:

$$\sigma_n(x) = K_n \Delta w(x) = K_n[w_2(x) - w_1(x)] \quad (27)$$

where $K_n$ is normal stiffness of the adhesive per unit length and can be deduced as $K_n = \frac{\sigma_n(x)}{\Delta w(x)} = \frac{\sigma_n(x)}{\Delta w(x)/s}\cdot\frac{1}{s} = \frac{E_a}{s}$, $E_a$ is Young's modulus in the adhesive; $\Delta w(x)$ is relative vertical displacement at the adhesive interface; $w_1(x)$ and $w_2(x)$ are vertical displacements of the concrete and the reinforcement, respectively.

Differentiating equation (27) twice results in:

$$\frac{d^2\sigma_n(x)}{dx^2} = K_n\left[\frac{d^2 w_2(x)}{dx^2} - \frac{d^2 w_1(x)}{dx^2}\right] \quad (28)$$

Considering the moment-curvature relationships for the beam to be strengthened and the external reinforcement, respectively:

$$\frac{d^2 w_1(x)}{dx^2} = -\frac{M_1(x)}{E_1 I_1}, \frac{d^2 w_2(x)}{dx^2} = -\frac{M_2(x)}{E_2 I_2} \quad (29)$$

where $I_1$ is section moment of inertia of R/C beam based on concrete and $I_2$ is section moment of inertia of external reinforcement.

Substituting equation (29) into equation (28) gives:

$$\frac{d^2\sigma_n(x)}{dx^2} = K_n\left[\frac{M_1(x)}{E_1 I_1} - \frac{M_2(x)}{E_2 I_2}\right] \quad (30)$$

Take the first derivation of x in equation (30) with the substitution of equation (5), (8) and we get:

$$\frac{d^3\sigma_n(x)}{dx^3} = K_n\left\{\left[\frac{V_1(x)}{E_1 I_1} - \frac{V_2(x)}{E_2 I_2}\right] + \left[\frac{1}{E_2 W_2} - \frac{e}{E_1 I_1}\right] b_2\tau(x)\right\} \quad (31)$$

Moreover, take the first derivation of x in equation (31) with the substitution of equation (4), (7), (13) and we get:

$$\frac{d^4\sigma_n(x)}{dx^4} = K_n b_2\left\{-\left(\frac{1}{E_1I_1}+\frac{1}{E_2I_2}\right)\sigma_n(x)+\alpha\left(\frac{1}{E_2W_2}-\frac{e}{E_1I_1}\right)\left[C_1\sinh(\alpha x)+C_2\cosh(\alpha x)\right]\right\}- K_n\rho b_1\left[\frac{1}{E_1I_1}+\left(\frac{1}{E_2W_2}-\frac{e}{E_1I_1}\right)\frac{K_s b_2}{\alpha^2 E_1W_1}\right] \quad (32)$$

Finally, the solution of equation (32) can be expressed as:

$$\sigma_n(x) = e^{-\beta x}\left[C_3\cos(\beta x)+C_4\sin(\beta x)\right]+e^{\beta x}\left[C_5\cos(\beta x)+C_6\sin(\beta x)\right]+C_7\sinh(\alpha x)+C_8\cosh(\alpha x)- \frac{K_n\rho b_1}{4E_1I_1\beta^4}\left[\frac{1}{E_1I_1}+\left(\frac{1}{E_2W_2}-\frac{e}{E_1I_1}\right)\frac{K_s b_2}{\alpha^2 E_1W_1}\right] \quad (33)$$

where $\beta = \left[\frac{K_n b_2}{4}\left(\frac{1}{E_1I_1}+\frac{1}{E_2I_2}\right)\right]^{\frac{1}{4}}$; Since we are dealing with small displacement problem and from a practical point of view, it is seen that $\sigma_n(x)$ can not become very large as $x$ becomes large, which requires that $C_5 = C_6 = 0$; $C_7 = \frac{\alpha K_n b_2\left(\frac{1}{E_2W_2}-\frac{e}{E_1I_1}\right)C_1}{\alpha^4+4\beta^4}$;

$C_8 = \frac{\alpha K_n b_2\left(\frac{1}{E_2W_2}-\frac{e}{E_1I_1}\right)C_2}{\alpha^4+4\beta^4}$; $C_3$ and $C_4$ can be determined by the boundary conditions at $x=0$ (equation (30), (31) ).

### (4) Determination of the axial force in FRP reinforcement under the given load or the applied load under the known axial force in FRP reinforcement

To obtain the accurate solution for a real structure, we adopt the nonlinear constitutive relationships for concrete and steel reinforcement in the composite beam (shown in **Fig. 7**). The FRP composites are assumed to behave linearly elastic up to failure. In the analysis, it is assumed that failure is reached when either the concrete strain reaches 0.0035 [4] or the FRP composites reach their ultimate strains.

When carrying the calculation of the applied load or the axial force in FRP reinforcement, the following assumptions are made:

(a) Linear strain distribution throughout the full depth of the section;

(b) No premature FRP separation or shear failure is accounted for, composite action is maintained up to failure;

(c) The tensile strength of the adhesive is ignored;

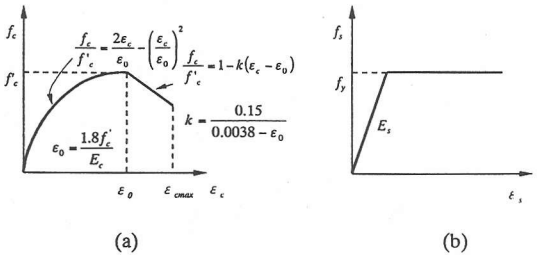


**Fig. 7** Constitutive relationship for materials: (a) concrete stress-strain curve, (b) steel stress-strain curve

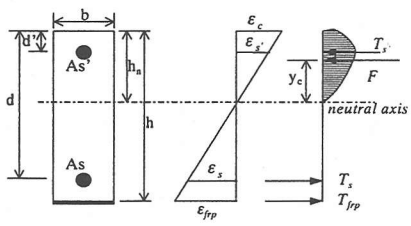


**Fig. 8** Analytical model based on strain compatibility

(d) Once crack occurs, no tension strength in concrete is assumed.

Based on the above assumptions and the analytical model illustrated in **Fig. 8**, an iterative procedure can be easily implemented in the computer program to determine the applied load with the known measuring position and tension strain of FRP or the axial force of FRP at the specific position when the applied load is known. The flow chart of calculating the axial force of FRP is shown in **Fig. 9**. In the program, each possible case is examined and the accurate solution to the structural response can be obtained.

## 3. VERIFICATION AND ILLUSTRATION OF THE DERIVED EQUATIONS

Some experimental studies consisting of three-point bending tests on several types of FRP-strengthened beams with and without steel reinforcement were carried out[1), 2), 3)]. To establish a rational design method for strengthening the RC beams with FRP, these experiments were focused on the observation of the debonding occurrence, crack propagation, failure modes, bond mechanism and the parametric studies (concrete strength, CFRP reinforcement, bond strength and steel reinforcing effect). There are two types of specimens in the experiment: notched and unnotched plain concrete beam strengthened with CFRP (Type I), CFRP-strengthened RC beam with and without stirrups and side-reinforcement (Type II). The details of the specimens are shown in **Fig. 10** and **Fig. 11**.

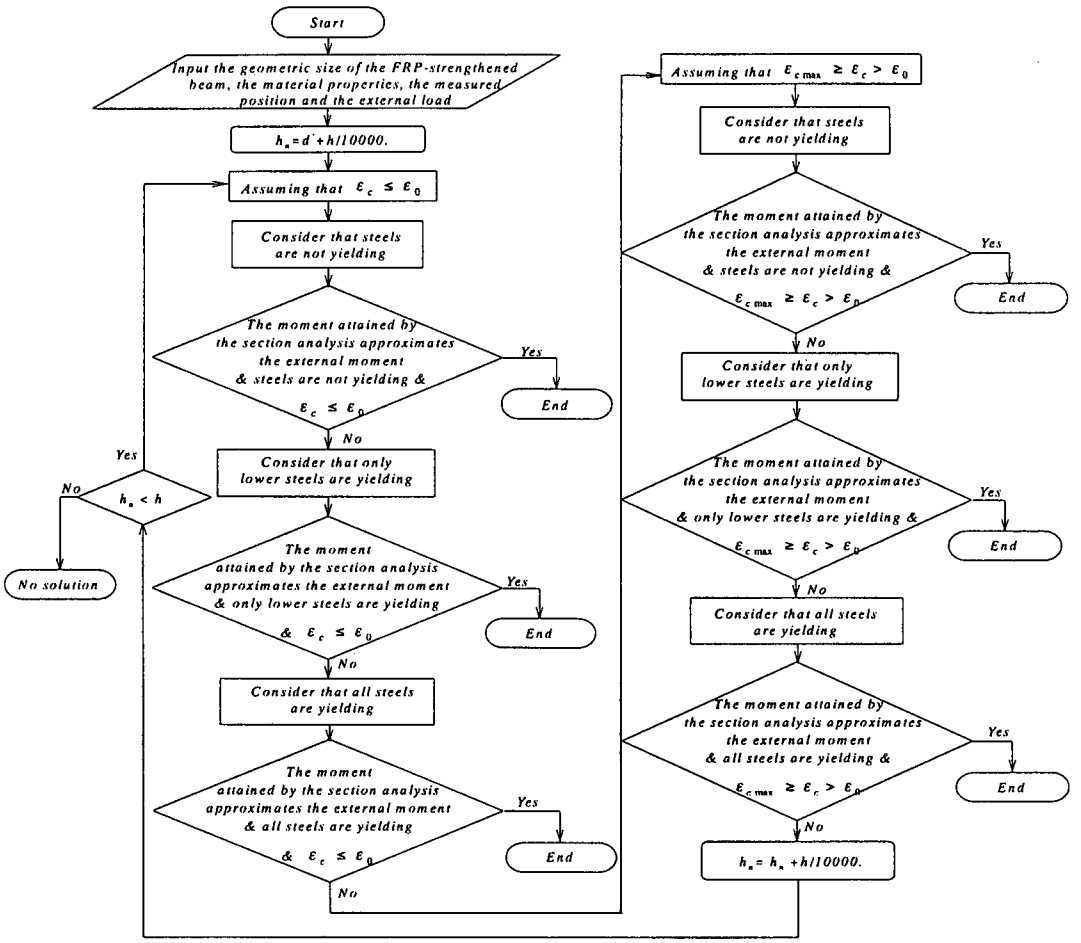


**Fig. 9** Flow chart of calculating the axial force of FRP when the load is known

**(1) Interfacial shear stresses for several load cases**

The notched plain concrete beam strengthened with FRP sheets is analyzed with the aforementioned derivations and the "ABAQUS" Finite Element program (ABAQUS, Version 5.8, 1998).

Due to the symmetry of the specimens, only half of the beam is analyzed with appropriate constraints at the centerline, as shown in **Fig. 12**. The FRP sheets are modeled as linear truss elements and the FRP-concrete interface is modeled as flexible joint element where linear spring behavior is used.

Based on the axial stress of FRP and the applied load calculated by ABAQUS, the interfacial shear stresses can be attained by the derived theoretical equations. Seen from the calculation results (**Fig. 13, Fig. 14, Fig. 15, Fig. 16**), the interfacial shear stresses at the flexural cracks show very high concentrations and this may lead to interfacial fracture propagation. It can be concluded that the gradient of the moment, or the shear force has an insignificant effect on the distribution of interfacial shear stresses for cracked FRP-strengthened beam. From **Fig. 13(b)**, **Fig. 14(b)** and **Fig. 15(b)**, it can be found that the interfacial shear stresses predicted by the derived theoretical equations agree well with the ones simulated by FEM in the case of lower shear stiffness of interface (According to Ref. 11), the shear stiffness of interface is generally of the order of $1.50\times10^2$ MPa/mm. Therefore, the value of $K_s=1.50\times10^2$MPa/mm is adopted here) and they appear some differences from FEM prediction only within a short distance around cracks in the case of higher stiffness of interface (To give an example, if the shear modulus of the adhesive layer is taken the value of the epoxy, i.e. $G_a=3.43\times10^3/(2\times(1+0.35))\approx1.27\times10^3$MPa, and the thickness of the adhesive layer is taken the value of s=0.89mm by considering 1.0mm as total thickness of regular FRP-resin system, the stiffness of interface is $K_s=G_a/s=1.43\times10^3$MPa/mm). Although there are slightly more deviations between the two results, the overall predication effect and the maximum shear stresses at the locations of the cracks which are the focuses in

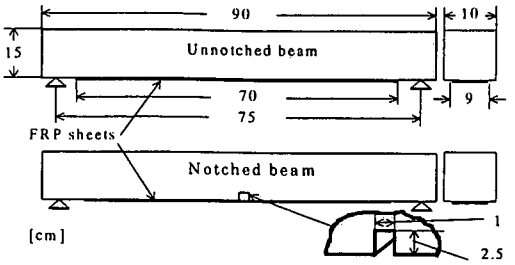


**Fig.10** Details of specimens for Type I

**Table 1** Material properties for Type I

| | | |
|---|---|---|
| concrete | Young's modulus [MPa] | $2.15\times10^4$~$3.53\times10^4$ |
| | compressive strength [MPa] | 24.5, 39.2, 53.9 |
| | Poisson's ratio | 0.16 |
| | slump [m] | 0.08, 0.105 |
| CFRP sheets | Young's modulus [MPa] | $2.30\times10^5$ |
| | tensile strength [MPa] | $3.2\times10^3$ |
| | thickness [cm] | 0.011 |
| | Poisson's ratio | 0.3 |
| epoxy | Young's modulus [MPa] | $3.43\times10^3$ |
| | Poisson's ratio | 0.35 |

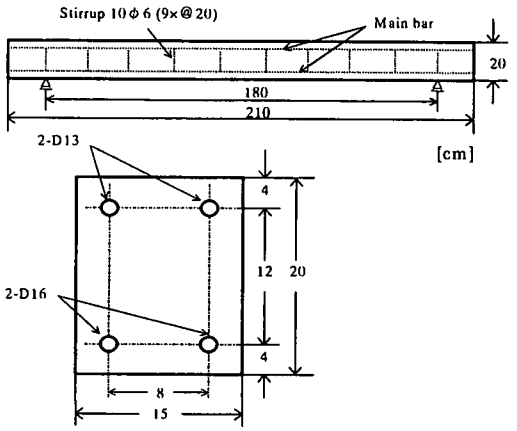


**Fig. 11** Details of specimens for Type II

**Table 2** Material properties for Type II

| | | |
|---|---|---|
| concrete | Young's modulus [MPa] | $3.15\times10^4$ |
| | compressive strength [MPa] | 30.2 |
| | Poisson's ratio | 0.16 |
| | slump [m] | 0.10 |
| CFRP sheets | Young's modulus [MPa] | $2.30\times10^5$ |
| | tensile strength [MPa] | $3.2\times10^3$ |
| | thickness [cm] | 0.011 |
| | Poisson's ratio | 0.3 |
| steel | Young's modulus [MPa] | $2.1\times10^5$ |
| | Yielding strength [MPa] | 420 |
| epoxy | Young's modulus [MPa] | $3.43\times10^3$ |
| | Poisson's ratio | 0.35 |

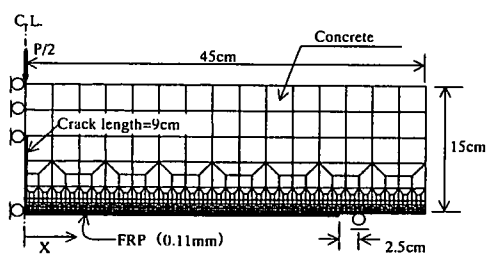


(a) General mesh of the test beam

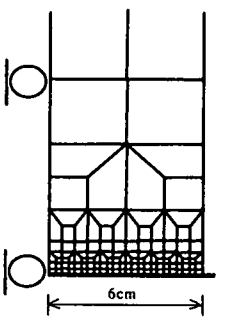


(b) Detailed mesh near the FRP-concrete interface

**Fig. 12** Mesh of the plain concrete specimen with initial crack (Type I)

this paper are in a relative good agreement to the results predicted by the finite element analysis.

### (2) Interfacial normal stresses along the FRP-concrete interface

The derived equation for calculating the normal stresses is verified by comparing it to Ref. 8) and FEM numerical simulation. Seen from **Fig. 17(b)**, it can be concluded that the interfacial normal stress at the location of the flexural crack does not show very high concentration as the shear stress does though the results attained by theoretical equation show much deviation from the finite element results, which indicate a slightly large compressive normal stress at the location of the flexural crack.

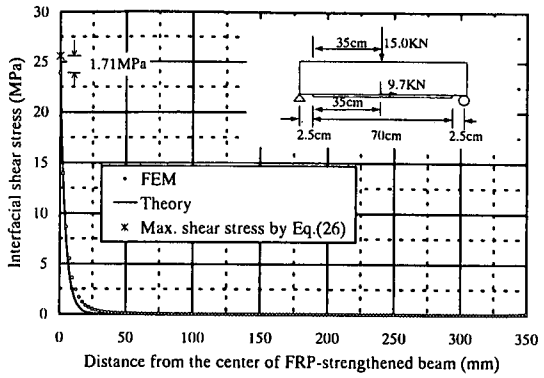


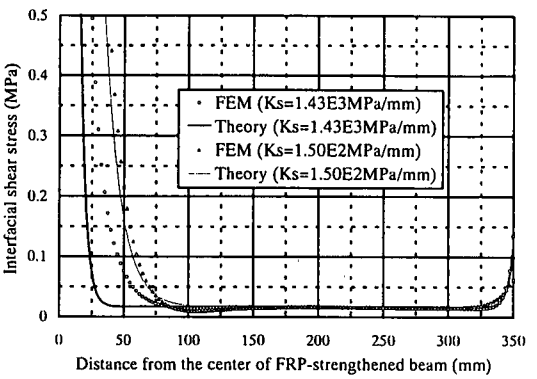


(a) Comparison of the derived formula to FEM (Ks=1.43×10³MPa/mm) (b) Magnification of the shear stress around the crack

**Fig. 13** Three-point bending case with unique flexural crack

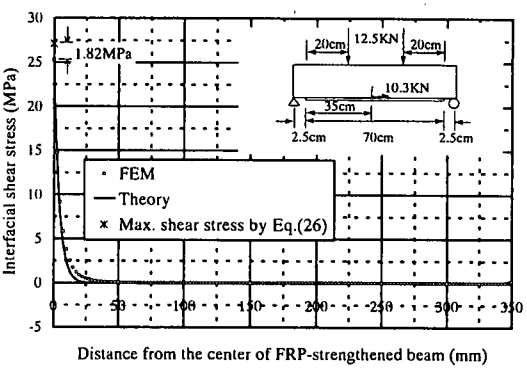


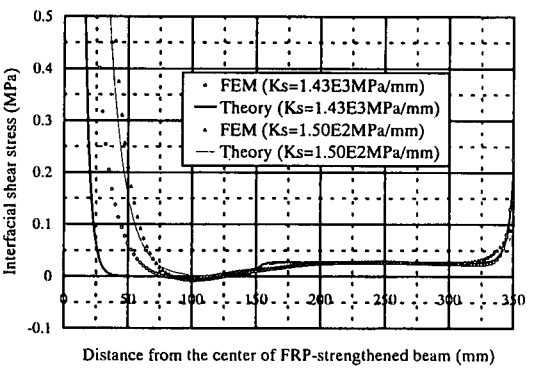


(a) Comparison of the derived formula to FEM (Ks=1.43×10³MPa/mm) (b) Magnification of the shear stress around the crack

**Fig. 14** Four-point bending case with unique flexural crack

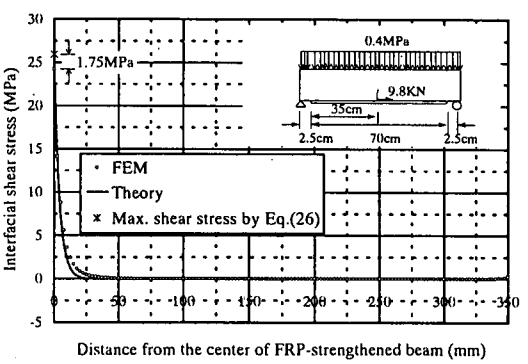


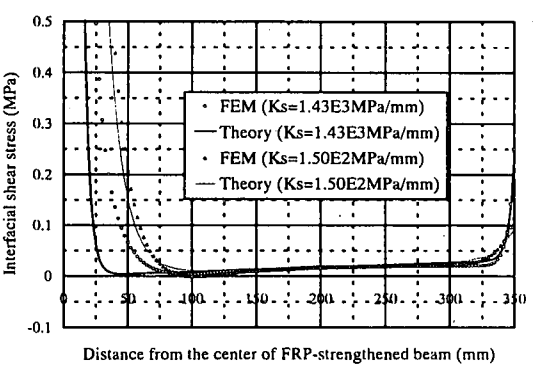


(a) Comparison of the derived formula to FEM (Ks=1.43×10³MPa/mm) (b) Magnification of the shear stress around the crack

**Fig. 15** Uniformly distributed loading case

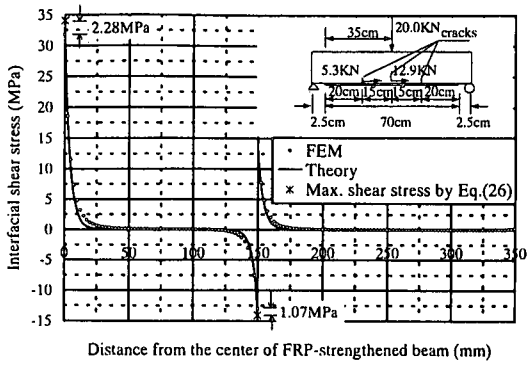


Fig. 16 With multiple flexural cracks (Ks=1.43×10³MPa/mm)

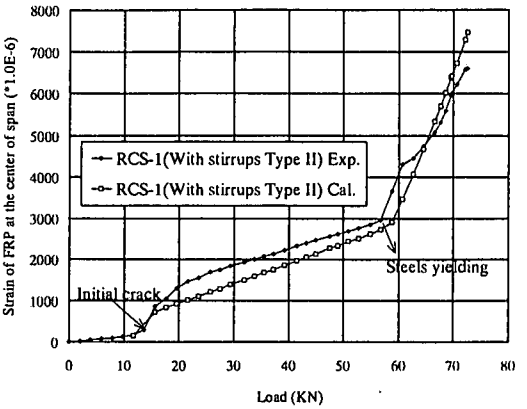


Fig. 18 Experimental result versus the calculated value

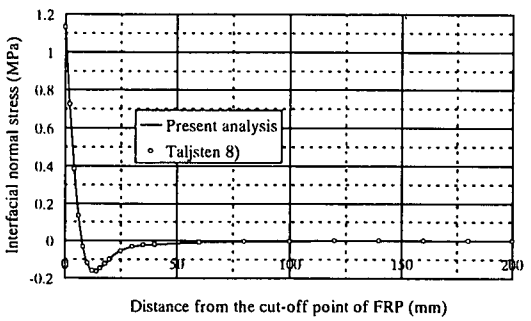


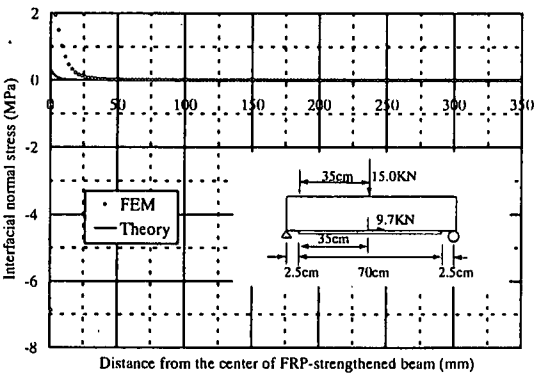


(a) Comparison of the derived formula to Täljsten (no crack) (b) Comparison of the derived formula to FEM (Ks=1.43×10³MPa/mm)

Fig. 17 Peeling stress along the three-point bending case

### (3) Structural response simulation of FRP-strengthened beams

The calculation method based on strain compatibility as stated in section 2.4 is used to analyze the experiment[2] and it is found that the calculation values match the experimental results in a high accuracy as shown in **Fig. 18**. Therefore it can be used for further investigation.

## 4. PARAMETRIC STUDIES

To gain an explicit understanding of the effects of the main design variables such as elastic modulus, thickness and width of FRP, shear modulus and thickness of the adhesive layer, distance from the support to the edge of the FRP sheet on the interfacial shear stresses of the composite beam with flexural cracks, a parametric study herein is conducted on the basis of the strain compatibility described in section 2.4. The notched beam shown in **Fig. 10** is used for the analysis.

Through the numerical calculation, the following conclusions can be drawn:

(1) The effective shear transfer length can be enlarged by increasing elastic modulus or thickness of FRP while the width of FRP nearly does not influence it (**Fig. 19**, **Fig. 20** and **Fig. 23**). So we can define the multiplication of elastic modulus and thickness of FRP as reinforcement stiffness for simplicity. Either increasing the reinforcement stiffness or the width of FRP will yield a higher load-carrying capacity against debonding failure.

(2) With decreasing the shear modulus or increasing the thickness of the adhesive layer, the effective shear transfer length also increases (**Fig. 21** and **Fig. 22**). However, the stiffness of the adhesive layer is considered to have no effect on the load-carrying capacity of the composite beam till to debonding. The effect of the adhesive layer can be regarded as mainly playing a role in transferring surely shear stresses from the concrete to the FRP sheet.

(3) Increasing the distance from the support to the edge of the FRP sheet only increases the

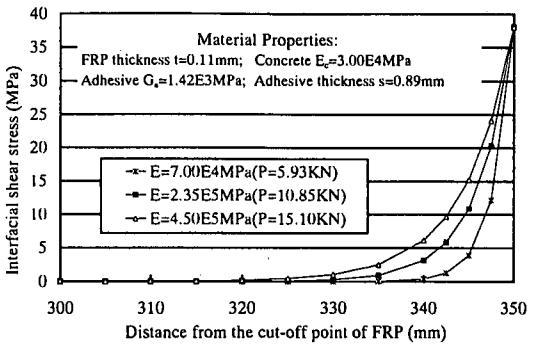


(a) Effect of elastic modulus on shear stress

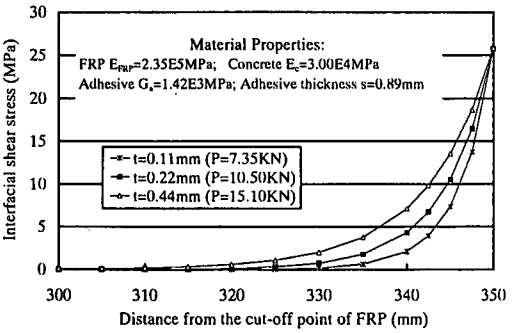


(b) Effect of thickness on shear stress

**Fig. 19** Variables of the FRP (Fixing the maximum shear stress at the end of flexural crack)

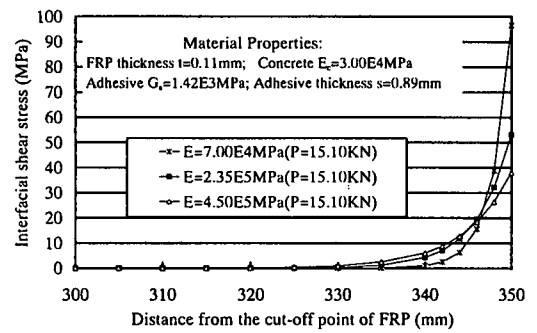


(a) Effect of elastic modulus on shear stress

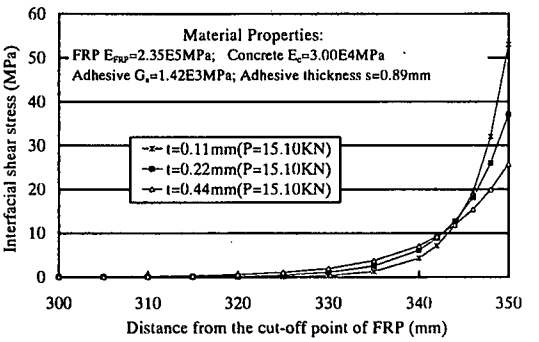


(b) Effect of thickness on shear stress

**Fig. 20** Variables of the FRP (Fixing the external load)

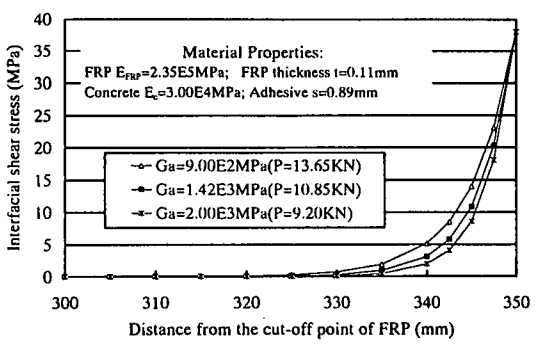


(a) Effect of elastic modulus on shear stress

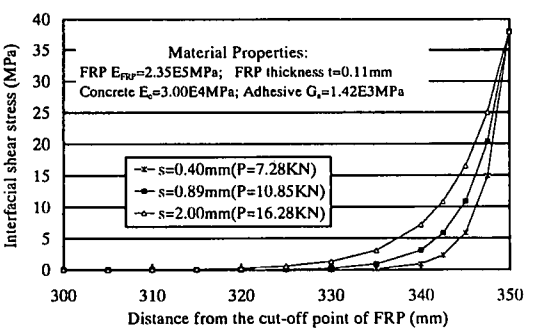


(b) Effect of thickness on shear stress

**Fig. 21** Variables of the adhesive (Fixing the maximum shear stress at the end of flexural crack)

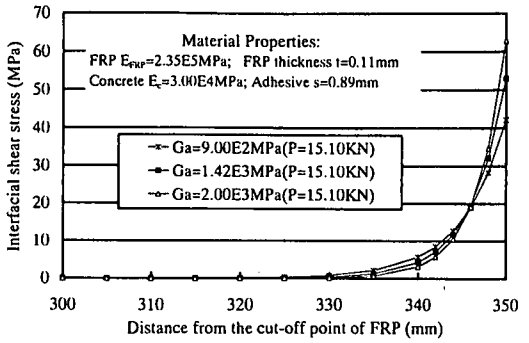


(a) Effect of elastic modulus on shear stress

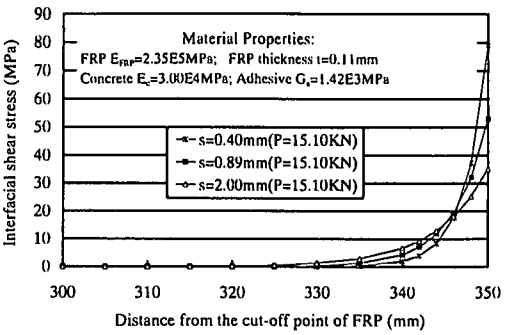


(b) Effect of thickness on shear stress

**Fig. 22** Variables of the adhesive (Fixing the external load)

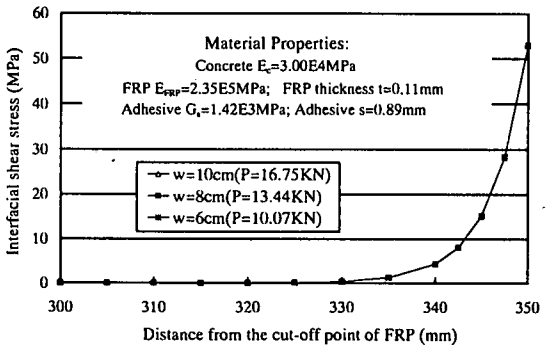


**Fig. 23** Effect of width of FRP on shear stress

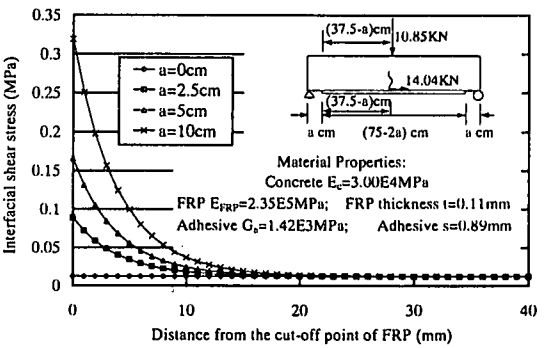


**Fig. 24** Effect of the distance from the support to the cut-off point of FRP on shear stress

interfacial shear stresses near the cut-off point (**Fig. 24**).

## 5. PROPOSED METHOD FOR PREDICTING THE INITIAL DEBONDING LOAD

### (1) Criteria for determining the initiation of debonding

Täljsten[12] applied linear fracture mechanics to the plate bonding technique and derived a series of formula based on the simplified shear-slip curve and the linear elastic assumption of the materials (**Fig. 25**). The derived expression for the interfacial shear stress can be written as:

$$\tau(x) = \frac{P_{max}\varpi}{b_2}\frac{\cosh(\varpi x)}{\sinh(\varpi l)},\quad 0 \le x \le l \tag{34}$$

where $b_2$ is the width of the FRP, $\varpi^2 = \frac{G_a}{s}\left(\frac{1}{E_1 t_1}+\frac{1}{E_2 t_2}\right)$, $s$ is the thickness of the adhesive, $G_a$ is the shear modulus in the adhesive, and $E_1 t_1$ and $E_2 t_2$ are the stiffnesses of concrete and FRP, respectively.

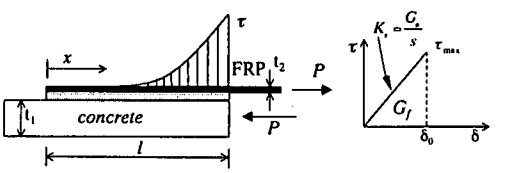


**Fig. 25** Simple shear test

The distribution of interfacial shear stresses is illustrated as shown in **Fig. 25**. Ignoring the minor term in equation (34), the shear stress at the end where the applied force is introduced can be attained from equation (35), which is same as equation (26) used for calculating the maximum interfacial shear stress near the flexural crack in the FRP-strengthened beam:

$$\tau(l) = \sqrt{\frac{G_a}{sE_2t_2}}\frac{P_{max}}{b_2},\text{(if } l \text{ is sufficiently large)} \tag{35}$$

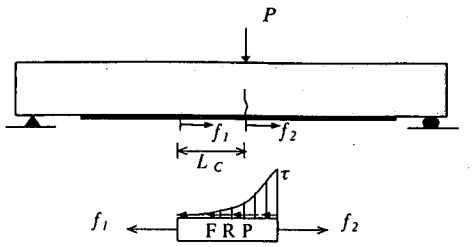


**Fig. 26** Investigation on the distribution of the axial force of FRP near the flexural crack

As stated before, the load-carrying capacity for a FRP-strengthened beam can be obtained by rewriting equation (26) as the following equation:

$$f_{max} = b_2 \tau_{max} \sqrt{\frac{sE_2t_2}{G_a}} \text{ or } \varepsilon_{max} = \tau_{max} \sqrt{\frac{s}{G_a E_2 t_2}} \qquad (36)$$

Seen from the calculation results (as shown in **Fig. 13** to **Fig. 17**), the flexural cracks located in maximum moment regions of the FRP-strengthened beam can initiate interfacial fracture propagation along FRP-concrete interface in strong shear (Mode II fracture based on the concept of fracture mechanics). The distribution of the interfacial shear stress is, to a large extent, dependent on the axial force of the FRP. Through the calculation of the FRP-strengthened beam using the program based on the RC beam theory, it is found that the axial force of FRP at a flexural crack is far lager than that at the uncracked location ($P$=15.10KN, $f_1$=19.56KN, $f_2$=0.48KN, $L_c$ =5cm) (**Fig. 26**).

Therefore, the stress conditions near the flexural crack of the FRP-strengthened beam can be regarded to be very similar to that of the simple shear test by ignoring the normal stresses. The debonding (interfacial crack) is initiated when the following equation is met:

$$|\tau_{max}| \geq \tau_f \qquad (37)$$

where $\tau_{max}$ is the maximum interfacial shear stress due to the flexural crack at the location of the maximum moment which can be calculated by equation (36); $\tau_f$ is the local shear strength of the adhesive layer (interface) and can be determined by the simple shear test of FRP[13].

Based on the above criterion and the RC beam theory, the initial debonding load can be predicted by combining equation (36) with equation (37).

Using linear fracture mechanics, as shown in **Fig. 25**, equation (36) for the maximum FRP axial force can be rewritten as:

$$f_{max} = b_2 \sqrt{2G_f E_2 t_2} \text{ or } \varepsilon_{max} = \sqrt{\frac{2G_f}{E_2 t_2}} \qquad (38)$$

where $b_2$ is the width of FRP; $E_2$ is the Young's modulus of FRP; $t_2$ is the thickness of FRP; $G_f$ is the interfacial fracture energy consumed for the initial debonding of FRP sheets.

Therefore, there is another way to predict the initial debonding load for the FRP-strengthened beam. Provided that the interfacial fracture energy consumed for the initial debonding is known, the initial debonding load can be determined by combining the above equation (38) with the RC beam theory through which the relationship of the FRP axial force and the external load can be calculated. Recently, a few studies have been carried on how to measure the critical mode II strain energy release rate and identify the fracture energy[13), 14)]. Wu et al.[13)] carried the identification of the fracture energy for CFRP-concrete interface through the experimental results of simple shear specimens. Fukuzawa et al.[14)] confirmed that the critical strain energy release rate along the CFRP-concrete (or mortar) interface could be measured using double-shear specimens pulled in tension. For lack of the data used for determining the initial debonding of the FRP-strengthened concrete beams, it is necessary to carry the identification of the interfacial fracture energy for initial debonding through the existing experiments.

**(2) Identification of maximum interfacial shear stress and interfacial fracture energy for initial debonding**

In **Table 3**, the maximum interfacial shear stress and the interfacial fracture energy consumed for the initial debonding in the experiments[2), 3)] are identified based on equations (36), (38) where the axial force of FRP is calculated by the RC beam theory (detailed information in section 2.4). It should be addressed that the initial debonding in the experiments was judged by bare eyes. In a strict sense, the initial debonding here is different from the definition of equation (37), but it can be considered as an evident (macroscopic) initiation of FRP debonding. It may be more important to predict the macroscopic initiation of debonding for practical application. Through the identification of the experimental results, the following conclusions can be made:

(1) By adopting linear shear stress-slip constitutive relationship, the maximum shear stress varies in the same way as the interfacial fracture energy and there exists a one-to-one corresponding relationship between them for a given value of the stiffness of the adhesive layer. So either of them can be used to determinate whether the

**Table 3** Summary of the experimental results and calculation of interfacial shear stress and fracture energy(Ks=1.43×10³MPa/mm)

| Specimen Types | | Concrete strength $f_c$ (MPa) | FRP characteristics | | | Exp. initial debonding load (KN) | Tensile force in FRP based on exp. data (KN) | Theoretical Maximum interfacial shear stress (MPa) | Identified interfacial fracture energy consumed for initial debonding (N/mm) |
|---|---|---|---|---|---|---|---|---|---|
| | | | Layer num. | Width (cm) | Pretensioned stress (MPa) | | | | |
| RC-1 [2] | Without stirrups (Type II) | 30.2 | 1 | 14 | 0 | 65.0 | 28.76 | 42.88 | 0.82 (peeling of FRP due to shear cruck) |
| RC-2 [2] | Without stirrups (Type II) | 30.2 | 1 | 14 | 0 | 68.9 | 26.06 | 37.97 | 0.67 (peeling of FRP due to shear cruck) |
| RC beam strengthened with CFS[3] | With stirrups (Type II) | 43.5 | 2 | 15 | 0 | 65.7 | 46.46 | 45.13 | 0.93 (debonding of FRP due to flexural cruck) |
| RCS-1 [2] | With stirrups (Type II) | 34.6 | 2 | 14 | 0 | 72.2 | 47.63 | 49.75 | 1.12 (debonding of FRP due to flexural cruck) |
| Beam1 [3] | Prestressed CFS with stirrups and anchorage | 43.5 | 2 | 10 | 800 | 73.5 | 29.24 | 41.09 | 0.83 (debonding of FRP due to flexural cruck) |
| Beam2 [3] | Prestressed CFS with stirrups and anchorage | 43.5 | 2 | 10 | 800 | 81.5 | 35.72 | 51.09 | 1.23 (debonding of FRP due to flexural cruck) |
| Beam3 [3] | Prestressed CFS with stirrups and anchorage | 43.5 | 2 | 10 | 800 | 72.5 | 32.83 | 47.22 | 1.04 (debonding of FRP due to flexural cruck) |
| Beam4 [3] | Prestressed CFS with stirrups and anchorage | 43.5 | 2 | 10 | 800 | 80.2 | 32.76 | 46.26 | 1.04 (debonding of FRP due to flexural cruck) |
| RC-CP-1[2] | Prestressed CFS and without stirrups | 30.2 | 1 | 14 | 1066.7 | 74.5 | 27.65 | 40.16 | 0.75 (peeling of FRP due to shear crack) |
| RC-CP-2[2] | Prestressed CFS and without stirrups | 30.2 | 2 | 14 | 800 | 74.0 | 32.57 | 30.06 | 0.52 (peeling of FRP due to shear crack) |
| RC-CP-3[2] | Prestressed CFS and without stirrups | 30.2 | 2 | 14 | 640 | 78.4 | 35.20 | 32.69 | 0.61 (peeling of FRP due to shear crack) |
| RCS-CP-1[2] | Prestressed CFS and with stirrups | 34.6 | 2 | 14 | 800 | 85.0 | 42.26 | 41.95 | 0.88 (No initial debonding is observed) |

initial debonding occurs or not.

(2) The identified maximum shear stress for the initial debonding is ranged from 41.09MPa to 51.09MPa (Ks=1.43 × 10³MPa/mm) and the interfacial fracture energy consumed for initial debonding is ranged from 0.83N/mm to 1.23N/mm. For the peeling case due to shear cracks of concrete, the maximum shear stress is 30.06MPa ~ 42.88MPa (Ks=1.43×10³MPa/mm) and the fracture energy is 0.52N/mm~0.82N/mm.

(3) It is found that the maximum shear stress and the interfacial fracture energy for the peeling case due to the shear cracks of concrete are lower than those for the debonding case due to the flexural cracks of concrete. This may be due to the effect of model I fracture in the peeling case.

(4) In **Table 3**, the identified maximum shear stresses are considered to be comparatively larger than the real values observed from a simple shear test. This is induced by linear elastic assumption as shown in **Fig. 25** that can be applied until the certain area of debonding propagation where a certain inelastic zone has been formed already. If we need to capture the local shear stresses rationally, a nonlinear constitutive law for the adhesive layer (interface) such as bilinear softening model should be taken into consideration. Considering that the variation of the local shear strength does not influence the debonding load level if the area below the shear stress-slip curve (i.e. the interfacial fracture energy consumed for the initial debonding of FRP sheets) is kept constant, the identified values of the interfacial fracture energy for initial debonding in this paper can be applied to evaluate the debonding initiation load of the FRP-strengthened beams.

## 6. CONCLUSIONS

Much research work has been done on the local failure of the steel/FRP-strengthened R/C beam at the end of steel/FRP plate. However, the debonding due

to shear stress concentrations at flexural cracks is often observed in the experiments and it is considered to be more important in the design of R/C beams strengthened with epoxy bonded FRP sheets. Based on linear elastic theories, shear stresses along FRP-concrete interface with consideration of flexural cracks of concrete are predicted and verified by comparisons with FEM analyses. Through investigation on shear stress distribution between flexural beams and a single-lap shear test, a methodology for predicting the load of initial debonding (debonding initiation) is developed and can be included in the future design guideline.

## REFERENCES


1) Wu, Z. S., Matsuzaki, T. and Tanabe, K.: Experimental study on fracture mechanism of FRP-reinforced concrete beams, *Symposium on Non-Metallic (FRP) Reinforcement for Concrete Structures*, Japan Concrete Institute, pp.119-126, May, 1998 (In Japanese).
2) Wu, Z. S., Matsuzaki, T., Fukuzawa, K. and Kanda, T.: Strengthening effects on RC beams with externally prestressed carbon fiber sheets, *Journal of Materials, Concrete Structures and Pavements*, JSCE, No.641/V-46, pp.153-165, February, 2000 (In Japanese).
3) Wu, Z. S., Matsuzaki, T., Yokoyama, K. and Kanda, T.: Retrofitting method for reinforced concrete structures with externally prestressed carbon fiber sheets, *Fourth International Symposium on Fiber Reinforced Polymer Reinforcement for Reinforced Concrete Structures*, ACI International, SP-188, pp.751-765, 1999.
4) Quantrill, R. J., Hollaway, L. C., and Thorne, A. M.: Experimental and analytical investigation of FRP strengthened beam response: Part I, *Magazine of Concrete Research*, Vol. 48, No. 177, pp.331-342, December, 1996.
5) Roberts, T. M.: Approximate analysis of shear and normal stress concentrations in the adhesive layer of plated RC beams, *The Structural Engineer*, vol. 67, No. 12, pp.229-233, 20 June, 1989.
6) Ziraba, Y. N., Baluch, M. H., Basunbul, I. A., Sharif, A. M., Azad, A. K., and Al-Sulaimani, G. J.: Guidelines toward the design of reinforced concrete beams with external plates, *ACI Structural Journal*, Vol. 91, No. 6, pp.639-646, November-December, 1994.
7) Quantrill, R. J., Hollaway, L. C., and Thorne, A. M.: Predictions of the maximum plate end stresses of FRP strengthened beams: Part II, *Magazine of Concrete Research*, Vol. 48, No. 177, pp.343-351, December, 1996.
8) Täljsten, B.: Strengthening of beams by plate bonding, *Journal of Materials in Civil Engineering*, ASCE, Vol. 9, No. 4, pp.206-212, November, 1997.
9) Malek, A. M., Saadatmanesh, H., and Ehsani, M. R.: Prediction of failure load of R/C beams strengthened with FRP plate due to stress concentration at the plate end, *ACI Structural Journal*, Vol. 95, No. 1, pp.142-152, January-February, 1998.
10) El-Mihilmy, M.: *Design and Behavior of Reinforced Concrete Beams Strengthened with Fiber-reinforced Plastics (FRP)*, Ph.D. thesis, Auburn University, Alabama, USA., August, 1998.
11) Nishida, H., Kamiharako, A., Shimomura, T. and Maruyama, K.: Bond mechanism between continuous fiber and concrete, *Proceedings of the Japan Concrete Institute*, Vol. 21, No. 3, pp.1507-1512, 1999 (In Japanese).
12) Täljsten, B.: Strengthening of concrete prism using the plate-bonding technique, *International Journal of Fracture Mechanics*, Vol. 82, pp.253-266, 1996.
13) Wu, Z. S., Murayama, D. and Yoshizawa, H.: An experimental study on bonding behavior and its improvement approach of CFRP sheets in anchorage zone, *Proceedings of the Japan Concrete Institute*, Vol. 21, No. 2, pp.211-216, 1999 (In Japanese).
14) Fukuzawa, K., Numao, T., Wu, Z. S., Yoshizawa, H. and Mitsui, M.: Critical strain energy release rate of interface debonding between Carbon Fiber Sheet and mortar, *Non-Metallic (FRP) Reinforcement for Concrete Structures, Proceedings of the Third International Symposium*, Vol. 1, pp.295-302, October, 1997.


**(Received December 22, 1999)**

# 曲げ部材におけるＦＲＰとコンクリートの接着界面のせん断応力伝達

呉　智深・牛　赫東

ＦＲＰシートや板のような面状補強材による接着補強工法の補強設計手法を確立するためには，理論的に検討すべき問題が数多く残されている．その中で，最も基本的問題と思われる接着界面の接着剥離特性が十分把握されたとは言い難い状態にある．例えば，コンクリート曲げ・せん断ひび割れの根本やＦＲＰ端部の応力集中より生じる各種剥離に対する評価・設計手法の構築は期待されている．本論文では，梁曲げ理論よりコンクリートひび割れを考慮したＦＲＰ－コンクリート接着界面の応力分布の解析式を導き，数値解析との比較検討を行った．また，単純付着試験体と曲げ部材のコンクリートひび割れ端部附近の接着界面せん断応力分布の比較検討により，曲げ部材の初期剥離算定手法を提案した．さらに幾らかのＦＲＰシートより補強されたＲＣ梁の試験結果により初期剥離時の最大せん断応力，剥離エネルギーを同定した．